www.acsnano.org

# Bioinspired and Low-Power 2D Machine Vision with Adaptive Machine Learning and Forgetting

Akhil Dodda, Darsith Jayachandran, Shiva Subbulakshmi Radhakrishnan, Andrew Pannone, Yikai Zhang, Nicholas Trainor, Joan M. Redwing, and Saptarshi Das\*



Downloaded via PENNSYLVANIA STATE UNIV on November 1, 2022 at 20:02:01 (UTC). See https://pubs.acs.org/sharingguidelines for options on how to legitimately share published articles.

Cite This: https://doi.org/10.1021/acsnano.2c02906



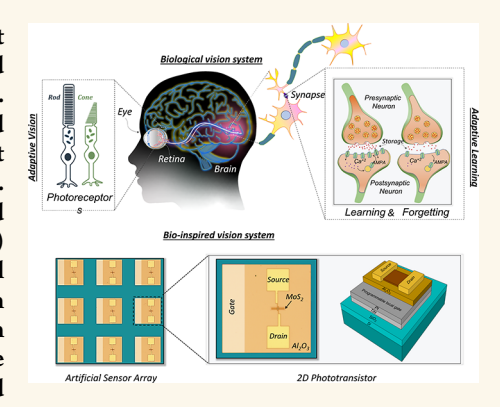
**ACCESS** I

Metrics & More

Article Recommendations

Supporting Information

ABSTRACT: Natural intelligence has many dimensions, with some of its most important manifestations being tied to learning about the environment and making behavioral changes. In primates, vision plays a critical role in learning. The underlying biological neural networks contain specialized neurons and synapses which not only sense and process visual stimuli but also learn and adapt with remarkable energy efficiency. Forgetting also plays an active role in learning. Mimicking the adaptive neurobiological mechanisms for seeing, learning, and forgetting can, therefore, accelerate the development of artificial intelligence (AI) and bridge the massive energy gap that exists between AI and biological intelligence. Here, we demonstrate a bioinspired machine vision system based on a 2D phototransistor array fabricated from large-area monolayer molybdenum disulfide (MoS<sub>2</sub>) and integrated with an analog, nonvolatile, and programmable memory gate-stack; this architecture not only enables dynamic learning and relearning from visual stimuli but also offers learning adaptability under noisy



illumination conditions at miniscule energy expenditure. In short, our demonstrated "all-in-one" hardware vision platform combines "sensing", "computing", and "storage" to not only overcome the von Neumann bottleneck of conventional complementary metal-oxide-semiconductor (CMOS) technology but also to eliminate the need for peripheral circuits and sensors.

KEYWORDS: Two-dimensional materials, machine vision, bioinspired, low-power sensors, neuromorphic, phototransistor

ny intelligent system, natural or artificial, is one that monitors its environment, learns or remembers key information, and adapts to changes as necessary. Animals do this seamlessly, often with very limited resources and in challenging ecological conditions. Their success can be attributed to the underlying biological neural networks (BNNs) that not only correlate and collocate the neural primitives for "sensing", "computing", and "storage", which drastically reduces the energy expenditure for many difficult tasks, but also learn and adapt, thus ensuring the survival of the species even in the most resource-constrained environments.

The world we "know" is a result of the perception enabled by our sensory organs. Information embedded in the outside world takes multiple sensory pathways, and their associated transformations, before it reaches the brain, which then processes it to give a wide variety of outcomes and sensations, aiding in learning and memory formation. In primates (including humans), vision constitutes a major portion of information input, more than all the other sensory inputs combined. Hence, a substantial percentage of the brain is devoted for processing visual stimuli, highlighting the importance of visual systems in learning.<sup>1</sup>

Drawing inspiration from the biological intelligence observed in visual animals, machine learning and machine vision are pushing the limits of artificial intelligence (AI) in our everyday lives, from defeating professional players in the game of "Go"<sup>2</sup> to driving autonomous vehicles in crowded streets.<sup>3</sup> Recent years have seen significant progress in artificial neural networks (ANNs),<sup>4</sup> which are high-level abstractions of BNNs, i.e., neurons connected to other neurons through synapses. Software-based ANNs and their different incarnations, such as deep neural networks (DNNs),<sup>5</sup> convolution neural networks

Received: March 24, 2022 Accepted: October 14, 2022



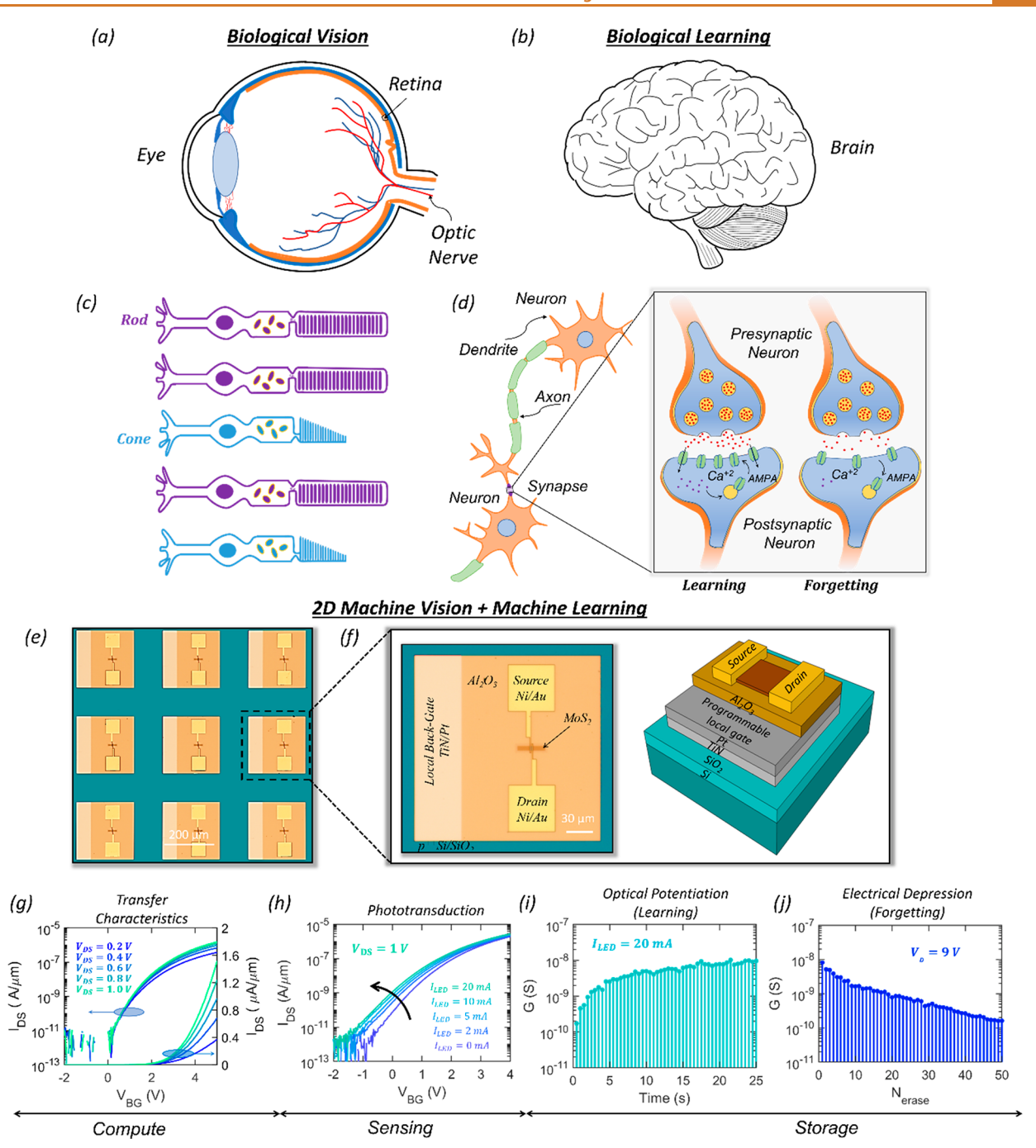


Figure 1. Bioinspired 2D vision system. Elementary components of a biological visual neural network: (a) eyes enabling biological vision and (b) visual cortex in the brain enabling biological learning. (c) Photoreceptors in the eyes enable phototransduction and adaptation. Rods facilitate scotopic vision and cones enable photopic vision. (d) Synapses strengthen or weaken to learn or forget. (e) Optical image of the artificial vision system comprised of a 3  $\times$  3 2D phototransistor array. (f) Optical image and schematic of an individual monolayer MoS<sub>2</sub> phototransistor, which is locally gated using a back-gate stack composed of atomic layer deposition (ALD) grown 50 nm Al<sub>2</sub>O<sub>3</sub> on Pt/TiN/p<sup>++</sup>-Si. (g) Transfer characteristics, i.e., source-to-drain current ( $I_{DS}$ ) as a function of the back-gate voltage ( $V_{BG}$ ), at different drain biases ( $V_{DS}$ ) in the dark, (h) phototransduction under different levels of illumination from a blue light emitting diode (LED), (i) optical potentiation induced learning, or increase in device conductance (G), and (g) electrical depression induced forgetting, or decrease in G, measured at  $V_{BG} = 0$  V in a representative 2D phototransistor.

(CNNs),<sup>6</sup> and, more recently, biorealistic and event driven spiking neural networks (SNNs),<sup>7</sup> have shown remarkable success in multiple applications, including image processing, pattern classification, and solving complex optimization problems. Their hardware implementation has primarily relied on conventional Si-based complementary metal-oxide-semiconductor (CMOS) technology.<sup>8–10</sup> However, unlike BNNs,

where the "computing" primitives, i.e., neurons, and synapses (storage units) are collocated, the von Neumann architecture used by Si CMOS physically separates "compute" from "memory", leading to orders of magnitude higher energy expenditure compared to what the brain requires for similar tasks. <sup>11–13</sup> Non-von Neumann computing architectures based on field-programmable gate arrays (FPGAs)<sup>14</sup> and resistive

random-access memory (RRAM)<sup>15–20</sup> bridge the gap between "memory" and "compute", thus offering energy efficient alternatives for hardware implementation of ANNs. However, current iterations of these in-memory compute architectures heavily rely on CMOS-based peripheral sensors and circuits, adding significant area and energy overhead. <sup>12,13,21–23</sup>

In contrast to the silicon and memristor based efforts, early machine vision advancements primarily relied on developing better photodetectors and, in some instances, integrating CMOS-based preprocessing modules (image filters, feature extractors, etc.) to bridge the gap between "sensing" and "compute". 24-28 More recently, researchers in the area of brain-inspired machine vision have also attempted to combine "sensing" with "memory". 13,23,29 While some of these demonstrations exploit oxide-based 30-32 and organic memristors,<sup>33</sup> perovskites,<sup>34–36</sup> etc., two-dimensional (2D) semiconducting monolayers are receiving significant attention due to their superior photosensitivity, 37,38 gate-tunability, 39,40 scalability, <sup>41</sup> and ease of integration with Si-based memory technologies. <sup>42–47</sup> Utilizing these advantages, researchers have shown machine learning in hardware via back-propagation algorithms implemented using software ANNs, as well as MNIST digit recognition and filtering of preprocessed images using hardware ANNs. For example, Mennel et al.<sup>37</sup> exploited gate tunable photoconductivity in a WSe2-based photodiode array for image sensing and processing, Hong et al.<sup>36</sup> exploited the photogating effect in a MoS<sub>2</sub>/perovskite heterostructure to demonstrate spectral sensing, and Hou et al.<sup>35</sup> used a complex multilayer heterostructure to learn input patterns. However, these efforts still lack proper integration with sensing and storage, and they are unable to adequately adapt to noisy environmental conditions. Thus, none of the emerging vision platforms have successfully integrated "sensing", "compute", and "memory" for adaptive machine vision and learning through forgetting using a single hardware platform. A qualitative assessment of recent vision platform works is presented using a benchmarking table in Supporting Information 1.

Finally, while learning has been a topic of extensive research, the importance of forgetting in learning has not received adequate attention. Most researchers consider forgetting as a passive brain process that allows unused memories to disappear over time. However, this decades-old hypothesis has now been challenged by a radical idea that suggests that the brain is built to forget, not remember. In other words, forgetting is an active brain process that plays an important role in biological learning.

In light of the above discussion, it is imperative that the next generation of AI benefits from an integrated hardware platform that combines machine vision with machine learning via mimicking the adaptive neurobiological architectures for seeing, learning, and forgetting. Here, we accomplish the same by integrating a monolayer MoS<sub>2</sub> phototransistor array with an analog, nonvolatile, and programmable memory gatestack to bridge the gap between "sensing", "compute", and "storage". In short, we combine the analog optical memory observed in 2D phototransistors with the analog electrical memory enabled by the back-gate stack for memoryaugmented reinforcement learning, or "learning", and learning through forgetting, or "dynamic learning", from visual stimuli. Our bioinspired hardware vision platform also enables adaptive learning under noisy illumination conditions at miniscule energy expenditure, bridging the energy gap between AI and

natural intelligence. Supporting Information 2 shows a detailed comparison of the energy performance of our work with conventional Si-based CMOS. Finally, our "all-in-one" vision platform not only overcomes the von Neumann bottleneck of CMOS-based ANNs but also eliminates the need for CMOS-based peripheral sensors and circuit components.

The motivation behind using monolayer MoS<sub>2</sub> as the material for our bioinspired hardware vision platform is multifold. First, the realization of BNNs requires the involvement of photosensitive materials with unique properties to perform machine vision operations such as analog sensing and adaptation. Direct-bandgap monolayer 2D materials with their superior photosensitivity, and electrostatic gate tunability, are, therefore, natural choices for the next generation of bioinspired machine vision platforms. 49 Second, the atomically-thin nature of 2D monolayers allows for aggressive dimension scaling, hence enabling high integration density as reported recently. 41,50 Moreover, some of the early criticism of 2D materials have also been successfully addressed through the realization of low contact resistances, 51 high ON currents, 52 integration of ultrathin and high-k gate dielectrics,<sup>53</sup> and wafer scale growth, 54,55 making them a technologically viable option. Demonstration of 2D-based microprocessors, 56 analogue operational amplifiers,<sup>57</sup> and RF electronics components<sup>58</sup> support this claim. Finally, unlike silicon CMOS, 2D materials enable flexible<sup>59</sup> and printable<sup>60</sup> electronic circuits, adding value toward 2D-based bioinspired and neuromorphic hardware platforms. 61-64

#### **RESULTS AND DISCUSSION**

Figure 1 illustrates the biological resemblance and functional capabilities of our hardware vision platform. Figure 1a-d show the visual BNN in humans and its associated neural primitives for seeing and learning. Information in the outside world is conveyed through images, which are projected by the lens system of the eyes into the retina (Figure 1a). Photoreceptors also transduce visual information into electrical impulses; with the help of other cells in the retina, these impulses pass on to the visual cortex in the brain (Figure 1c). The visual cortex contains a vast network of neurons which take part in learning. While the neuroscience of learning is still a topic of active research, it is widely accepted that learning leads to a strengthening of connections between associated neurons through a process known as synaptic plasticity (Figure 1d).<sup>65</sup> For example, long-term potentiation, or memory formation, leads to an increase in the number of AMPA receptors in the postsynaptic neuron when the presynaptic neuron uses glutamate as the neurotransmitter. 66 Similarly, forgetting leads to a weakening of connection strengths through a reduction in the number of AMPA receptors. The mathematical construct of synaptic plasticity determines the biological learning rule, which is often categorized as unsupervised in the context of machine learning, though evidence of reward-based or reinforcement learning can also be found.<sup>67</sup> Figure 1e shows an optical image of our  $3 \times 3$  2D phototransistor array, and Figure 1f shows an optical image and schematic of an individual monolayer MoS2 phototransistor; as with all phototransistors used in this work, this device is locally gated using a back-gate stack composed of atomic layer deposition (ALD) grown 50 nm Al<sub>2</sub>O<sub>3</sub> on Pt/ TiN/p++-Si. As we will elucidate later, photoinduced carrier trapping at the MoS<sub>2</sub>/Al<sub>2</sub>O<sub>3</sub> interface enables analog optical memory in MoS<sub>2</sub> phototransistors, which can then be exploited

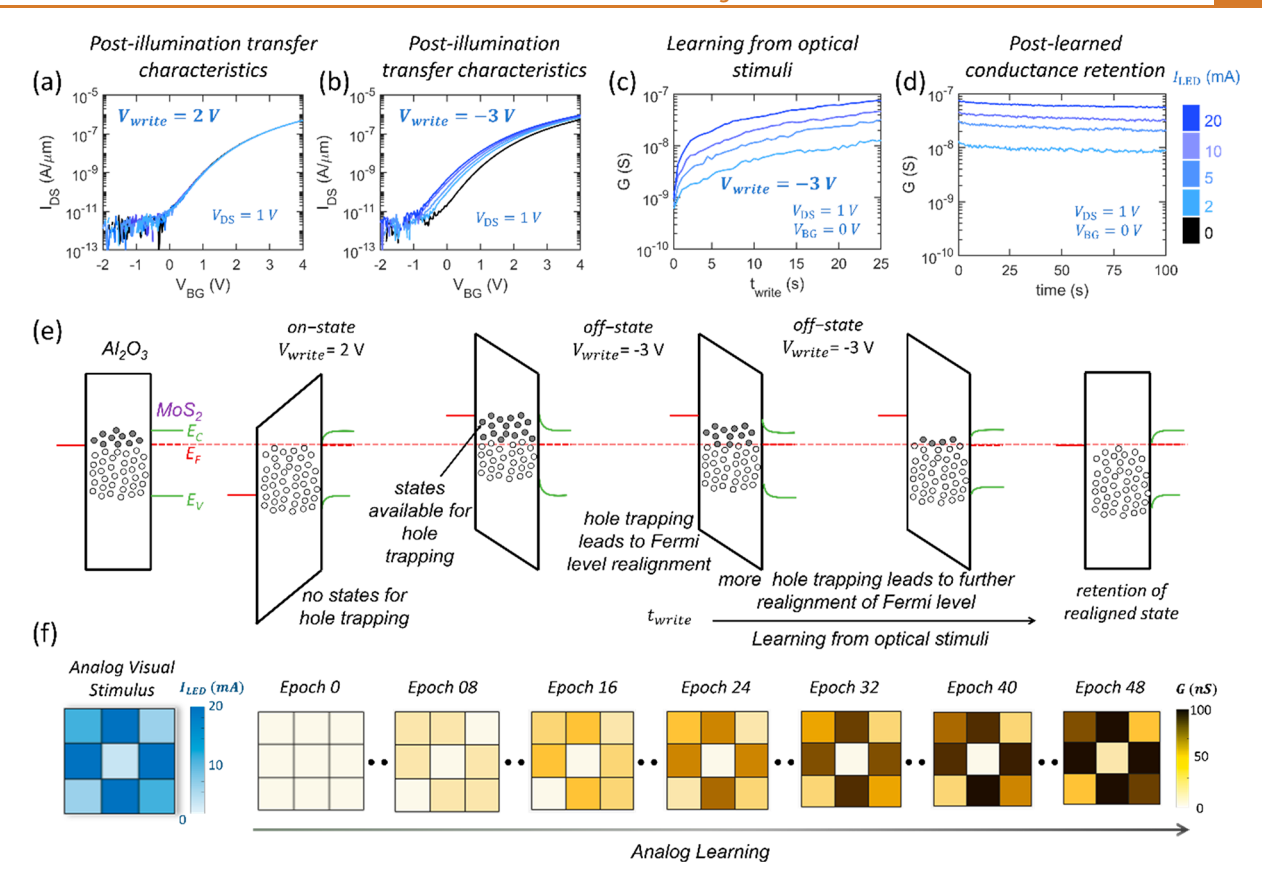


Figure 2. Analog vision and learning. Postillumination transfer characteristics of an MoS<sub>2</sub> phototransistor measured in dark after  $t_{\rm write}=10~{\rm s}$  exposure to blue LEDs at (a)  $V_{\rm write}=2~{\rm V}$  and (b)  $V_{\rm write}=-3~{\rm V}$  for different  $I_{\rm LED}$ . (c) Monotonic increase in conductance (G) measured at  $V_{\rm BG}=0~{\rm V}$  as a function of  $t_{\rm write}$  for different  $I_{\rm LED}$ . (d) Nonvolatile retention of the corresponding postillumination conductance states at  $V_{\rm BG}=0~{\rm V}$ . (e) Energy band diagrams for the MoS<sub>2</sub>/Al<sub>2</sub>O<sub>3</sub> interface under different  $V_{\rm write}$ , showing the dynamics of carrier trapping leading to persistent photoconductivity (optical memory). (f) Heatmaps of the input image, with each pixel corresponding to an  $I_{\rm LED}$  value, and the output images, with each pixel showing the G of the corresponding phototransistor in the 9 × 1 array measured at  $V_{\rm BG}=0~{\rm V}$ , at different epochs. The input image is learned in 50 epochs. This shows the analog vision and learning capabilities of the photoresponsive 2D array structure.

for direct and adaptive memory-augmented reinforcement learning from visual stimuli under different illumination conditions. On the other hand, analog electrical memory enabled by the programmable back-gate stack also allows for the realization of biological-equivalent forgetting, which facilitates learning through forgetting, as well as learning, under noisy illumination. Together, this stack enables adaptive vision and learning through in-memory sensing and computing, ultimately resembling the visual BNN in humans.

The monolayer MoS2 used in this study was grown via a metal-organic chemical vapor deposition (MOCVD) technique using a carbon-free chalcogen precursor at 1000 °C on an epitaxial sapphire substrate to ensure high film quality. Supporting Information 3a-c, respectively, show the atomic force microscopy (AFM) micrograph, Raman spectra, and photoluminescence (PL) spectra of a representative phototransistor in the vision platform. Following the growth, the film was transferred onto the local back-gate islands for the fabrication of the phototransistor array (see the Methods section for further details on synthesis, film transfer, and device fabrication). Figure 1g shows the transfer characteristics, i.e., source-to-drain current  $(I_{DS})$  as a function of the back-gate voltage  $(V_{\rm BG})$ , at different drain biases  $(V_{\rm DS})$  for a representative monolayer 2D phototransistor measured in the dark. The channel length (L) and width (W) of each device were 1 and 5  $\mu$ m, respectively. Supporting Information 4a-c, respectively, show the low device-to-device variation across the phototransistor array, as well as the output characteristics and back-gate hysteresis in a representative phototransistor. Figure 1h shows the response of the phototransistor to different levels of illumination from a blue light emitting diode (LED). Note that, instead of LASER illumination as used in most studies,<sup>3</sup> we have chosen LED illumination since it more closely simulates the natural lighting conditions wherein artificial vision sensors are deployed. Finally, Figure 1i-j, respectively, show optical potentiation induced learning, or increase in device conductance (G) under optical excitation, and electrical depression induced forgetting, or decrease in G due to electrical programming, measured at  $V_{\rm BG}$  = 0 V in a representative phototransistor, constructing the hardware foundation for artificial machine intelligence. Details of the optical potentiation and electrical depression are described in the following sections.

Direct and Analog Learning from Visual Stimuli Using 2D Phototransistor Array. Illumination of a 2D semiconducting channel in a phototransistor will generate photocarriers which, under an electrical bias, drift toward the respective electrodes, thus adding to the already existing dark current in the device. The illumination intensity will determine the change in the conductance of the channel, allowing one to

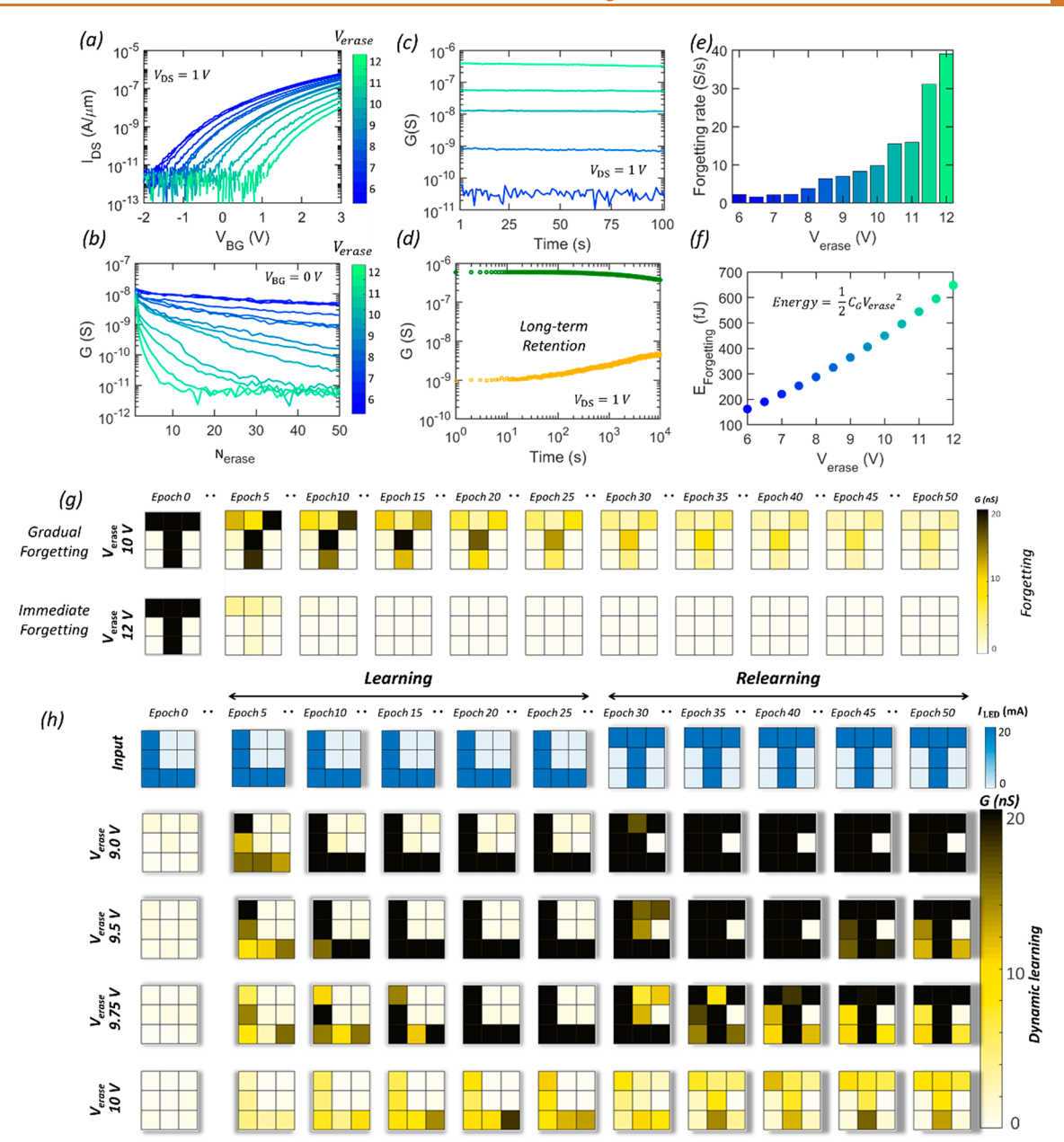


Figure 3. Forgetting for dynamic learning. (a) Transfer characteristics of a representative phototransistor when positive programming voltages ( $V_{erase}$ ) of increasing amplitude are applied to the back-gate, each for a total duration of 100 ms. (b) Device conductance (G) measured at  $V_{BG} = 0$  V as a function of the number of programming pulses ( $N_{erase}$ ) of pulse width  $t_{erase} = 100$  ms and of different amplitudes ( $V_{erase}$ ). (c) Nonvolatile retention of 5 representative postforgotten G-states measured at  $V_{BG} = 0$  V. (d) Long-term retention of two representative postprogrammed conductance states measured at  $V_{BG} = 0$  V for  $\sim 10^4$  s. (e) Forgetting rate, defined as the rate of decrease in G, for different  $V_{erase}$ , (f) Forgetting energy expenditure for different  $V_{erase}$ , (g) Heatmaps of G, showing that smaller amplitudes of  $V_{erase}$  = 0 V (top row) enable gradual forgetting of the learnt letter "T" while higher amplitudes of  $V_{erase}$ , e.g.,  $V_{erase} = 12$  V (bottom row), cause immediate forgetting. (h) Dynamic relearning enabled by adaptive forgetting. Heatmaps show learning of a letter "L" (first 25 epochs) and relearning of another letter "T" (final 25 epochs) by the phototransistor array with different forgetting rates. Here, each epoch consists of optical potentiation and electrical depression (application of  $V_{erase}$ ), enabling relearning and eliminating the need for supervision. The top row shows the input images ( $I_{LED}$ ). Each row below shows the corresponding heatmaps of G for different amplitudes of  $V_{erase}$ . Under optimum potentiation and depression (e.g.,  $V_{erase} = 9.75$  V), the phototransistor array can learn, forget, and relearn the input patterns.

leverage this property for analog machine vision sensors. In most cases, after the optical stimuli is removed, the conductance returns to the initial state without remembering the change induced by the stimuli. This is a limitation for many machine vision demonstrations, necessitating peripheral circuit elements to store the new conductance value induced by the optical stimuli.<sup>37</sup> This challenge is overcome via "optical memory", or persistent photoconductivity, which allows

materials/devices to remain in the new conductance state even after the visual stimuli is removed. In 2D-based vision sensors, this is mainly accomplished through trapping of photocarriers in trap states at the 2D semiconductor-oxide interface.  $^{37,44-46,63,68}$  These trapped charges alter the threshold voltage of the device, changing the conductance measured at a given  $V_{\rm BG}$ . The retention of this optically induced conductance state primarily depends on the detrapping time, which may

range from several hours to days. This particular phenomenon is called the photogating effect and is leveraged in our 2D-based machine vision platform to demonstrate direct learning from visual stimuli.

Figure 2a shows the postillumination transfer characteristics of a representative phototransistor at  $V_{DS} = 1 \text{ V}$  measured in the dark after  $t_{\text{write}} = 10 \text{ s}$  exposure to different illumination intensities  $(I_{LED})$  at  $V_{write} = 2$  V. Little-to-no change is observed in the device characteristics post illumination. However, as shown in Figure 2b, the postillumination transfer characteristics show a significant shift in the threshold voltage of the device when biased at  $V_{\text{write}} = -3 \text{ V}$  during the illumination. Supporting Information 5 and 6 show the influence of  $V_{\text{write}}$  in the dark and at different illumination intensities, respectively. Figure 2c shows the evolution of the postillumination conductance (G) of the phototransistor, when measured at  $V_{\rm BG}$  = 0 V, as a function of the LED illumination time ( $t_{\rm write}$ ) for different  $I_{LED}$ . Figure 2d shows the retention characteristics for G corresponding to different  $I_{LED}$  for a period of 100 s; these results suggest that the learned conductance states are stable over time. As mentioned earlier, these observations are attributed to the phenomenon of persistent photoconductivity, which is illustrated using the energy band diagrams in Figure 2e. At equilibrium, i.e., in the absence of any gate bias, the trap states with energy levels above the Fermi energy  $(E_{\rm F})$  are empty, whereas the ones below  $E_{\rm F}$  are filled. When the phototransistor is illuminated in the on-state or in the subthreshold region of device operation, most trap states are below  $E_{\rm F}$ , making carrier trapping unlikely; as a result, the device displays nonpersistent photoconductivity, i.e., the device returns to its initial state following illumination without any optical memory. However, when the phototransistor is illuminated in the off-state or in the depletion region of device operation, most trap states are above  $E_{\rm F}$ , thereby allowing carrier trapping at and/or near the MoS<sub>2</sub>/Al<sub>2</sub>O<sub>3</sub> interface. Negative shifts in  $V_{TH}$  indicate trapping of photogenerated holes. With longer illumination, more trap states are occupied, thus leading to more shifts in  $V_{\rm TH}$  with increasing  $t_{\rm write}$ . The detrapping process can be rather slow, leading to optically induced memory in the MoS<sub>2</sub> phototransistors. See Supporting Information 7 for the photogating effect as it corresponds to different wavelengths of light. As can be noted, irrespective of the wavelength used, we observe the photogating effect in our MoS<sub>2</sub> phototransistors.

Leveraging the merits offered by the photogating effect described above, we demonstrate memory-augmented reinforcement learning directly from the optical stimuli (Figure 2f and Supplementary Video 1). An analog image of size  $3 \times 3$ , composed of 4 different LED illumination intensities ( $I_{LED} = 2$ mA, 5 mA, 10 mA, and 20 mA), is presented pixel-by-pixel to the phototransistors in the 3  $\times$  3 array at  $V_{\text{write}} = -3$  V. See Supporting Information 8 for device-to-device variation in the photoresponse among the 9 devices in the phototransistor array. The conductance states G are read at  $V_{BG} = 0$  V successively for 50 epochs by sampling  $I_{DS}$  every 500 ms. All devices start from the same conductance state,  $G \approx 1$  nS at  $V_{BG}$ = 0 V. During each epoch, devices learn the input image by updating G. As expected, devices exposed to brighter intensities reach higher G compared to the devices exposed to lower intensities due to the difference in the photogating effect, as illustrated in Figure 2c. As a result, the heatmap of G (Figure 2e) mimics the contrast present in the input image at the end of the 50 epochs, suggesting direct learning by the  $3 \times$  3 phototransistor array from the analog visual stimuli. The total learning energy expenditure per pixel after 50 epochs was found to be miniscule at  $\sim$ 50 nJ. In addition to being low-power, Supporting Information 9 demonstrates the realization of gate-tunable adaptive sensing in our phototransistors, allowing for them to detect scotopic (low-light) intensities and achieve low-latency.

Adaptive Forgetting. Forgetting has traditionally been considered to be a passive brain process, ensuring that unused information fades over time so that neural resources can be reallocated for storing more important and newer information. When machines learn with unrestricted storage resources (e.g., cloud servers), forgetting is irrelevant. However, when storage capacity is either limited or not accessible, for example, in Internet of Things (IoT) edge devices deployed in remote locations, forgetting can play an active role in smart learning.

Forgetting is enabled in our phototransistors by exploiting the nonvolatile and analog programmability of our local backgate dielectric stack. Figure 3a shows the transfer characteristics of the phototransistor when positive programming voltages ( $V_{\rm erase}$ ) of increasing amplitude are applied to the back-gate, each for a total duration of 100 ms. During programming, the source and drain terminals are kept grounded. Also note that before programming the device is set at a high conductance state. Transfer characteristics clearly show a positive shift in  $V_{\rm TH}$  with increasing magnitude of  $V_{\rm erase}$ . See Supporting Information 10 for a detailed explanation of programmable memory using energy band diagrams.

Figure 3b shows the evolution of the G measured at  $V_{BG} = 0$ V as a function of the number of epochs, i.e., programming pulses  $(N_{\text{erase}})$  of pulse width  $t_{\text{erase}} = 100$  ms and of different amplitudes ( $V_{\text{erase}}$ ), over a total duration of 5 s. Note that, since electrical programming via the back-gate results in a positive shift of  $V_{\text{TH}}$ , G decreases with increasing  $N_{\text{erase}}$  and  $V_{\text{erase}}$ ; hence, this reduction in G can be exploited as synaptic depression (forgetting). Forgetting is also permanent, as shown in Figure 3c using nonvolatile retention of five representative postforgotten G-states measured at  $V_{BG} = 0$  V. We also examined long-term memory retention in two representative analog conductance states for  $\sim 10^4$  seconds, as shown in Figure 3d. These results indicate that the programmed states are retentive for a longer duration of time than that demonstrated in Figures 2d and 3c. Unlike biological forgetting, wherein humans have limited control, the forgetting rate of our vision platform, which we define as the rate of decrease in G, can be precisely controlled through  $V_{\rm erase}$ (Figure 3e). Figure 3f shows the forgetting energy expenditure for different  $V_{\text{erase}}$ , calculated as  $1/2C_{\text{G}}V_{\text{erase}}^2$ , where  $C_{\text{G}} = 9$  fF is the gate capacitance; for all tested  $V_{\mathrm{erase}}$ , the energy expenditure is in the range of hundreds of femtojoules. The conductance (G) heatmaps shown in Figure 3g and Supplementary Video 2 illustrate the forgetting of a learned "T" pattern at different rates enabled by  $V_{
m erase}$ . Clearly, at a higher magnitude of  $V_{\rm erase}$ , e.g.,  $V_{\rm erase}$  = 12 V, the phototransistor array forgets the letter "T" almost immediately ( $\sim$ 10 epochs), whereas lower magnitudes of  $V_{\text{erase}}$  enable gradual forgetting (>50 epochs). The energy expenditures for immediate and gradual forgetting were found to be ~0.75 pJ/pixel and 2.5 pJ/pixel, respectively. In addition to learning and forgetting, an important metric for phototransistor synapses is the paired-pulsed facilitation (PPF) and pairedpulsed depression (PPD). See Supporting Information 11 for

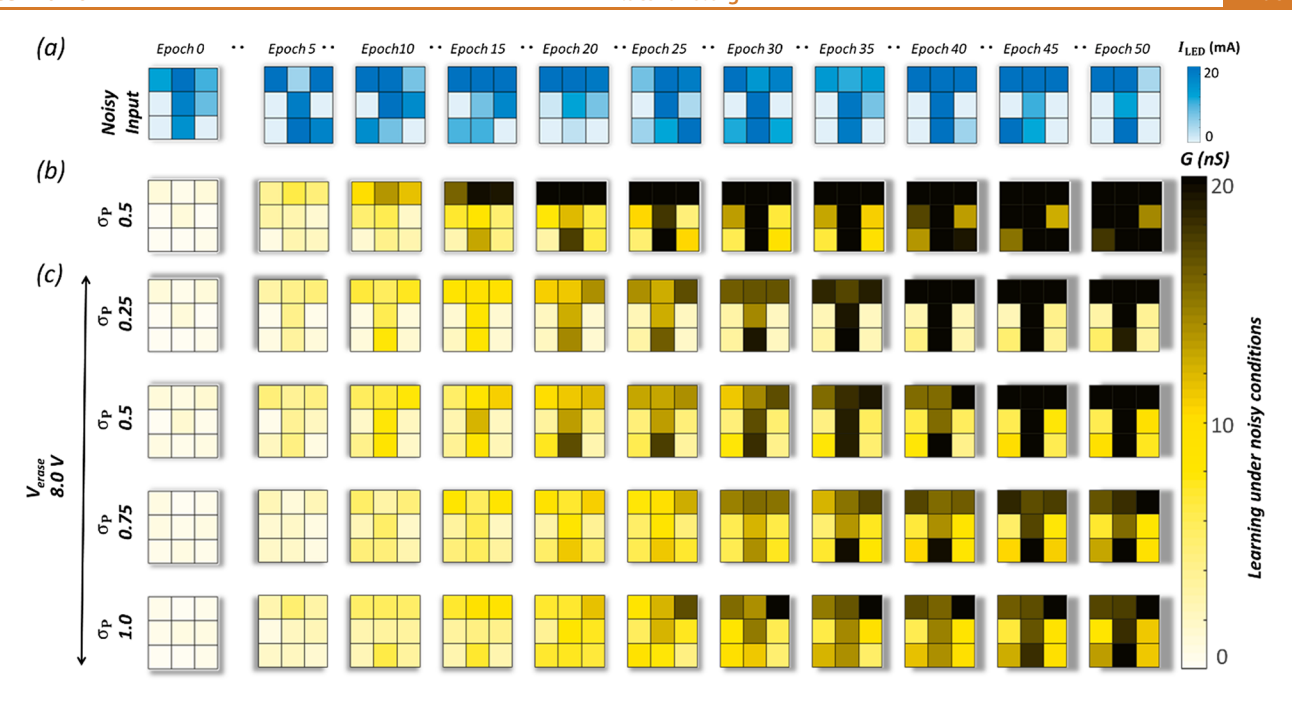


Figure 4. Learning under noisy conditions. (a) An example of noisy input images of the letter "T". To generate the noisy images, the input current to the LED corresponding to each pixel was superimposed with a zero mean white Gaussian random noise of standard deviations. Heatmaps of G measured at  $V_{BG} = 0$  V (b) without forgetting, i.e.,  $V_{erase} = 0$  V, and (c) with forgetting, i.e.,  $V_{erase} = 8.0$  V, for input images with noise of different standard deviations ( $\sigma_P = 0.25$ , 0.5, 0.75 and 1.0).

empirical models of PPF and PPD in our MoS<sub>2</sub>-based phototransistors and their corresponding index.

Importance of Forgetting in Dynamic Learning. Next, we elucidate the role of forgetting in dynamic learning, which refers to the process of automatic image update by removing the previously learnt image with an electrical voltage induced change in G. In this instance, each epoch consists of two cycles, optical potentiation for learning followed by electrical depression for forgetting. We have considered 3 × 3 pixel images of the letters "L" and "T" for learning and relearning, respectively, with each being presented for 25 epochs. As before, all devices were initially programmed to a low conductance state with  $G \approx 1$  nS. Figure 3h and Supplementary Video 3 show the time evolution of the heatmap of G during dynamic learning, i.e., sensing and storing the first image ("L") and gradually erasing it to store the new image ("T"), for different strengths of electrical depression obtained by using different  $V_{\rm erase}$ . Some of the key observations include: (1) If the strength of electrical depression is too weak (e.g.,  $V_{\text{erase}} = 9 \text{ V}$ ) compared to the optical potentiation, devices will never forget the learned pattern and relearning becomes futile. (2) If the strength of electrical depression is too strong (e.g.,  $V_{\text{erase}} = 10 \text{ V}$ ) compared to the optical potentiation, then it becomes difficult to learn any input pattern. 3) Under optimum potentiation and depression (e.g.,  $V_{\rm erase} = 9.75 \text{ V}$ ), the phototransistor array can learn, forget, and relearn the input patterns dynamically. These demonstrations illustrate the critical role of forgetting in dynamic learning.

Forgetting for Learning under Random Disturbance. Next, we show that forgetting plays an even more significant role when learning under noisy illumination conditions. Visual BNNs in humans possess the remarkable ability to identify important features in an image even in the presence of disturbances. For example, the brain remains able to extract information in poor weather conditions, such as mist, rain,

snow, and other impediments to perfect vision. Notably, this avoidance of dynamic noise remains a challenging task in machine vision systems, forcing them to rely on sophisticated computer algorithms for its elimination. As hardware implementations of such algorithms are naturally energy hungry, this can severely limit their implementation in resource-constrained environments. However, as we demonstrate below, forgetting can significantly aid in learning under dynamic noise, circumventing the need for such energyexpensive solutions. Figure 4 and Supplementary Video 4 show the time evolution of the heatmap of G measured at  $V_{BG} = 0 \text{ V}$ while learning from noisy  $3 \times 3$  pixel images of the letter "T" in the absence of (Figure 4b) and with (Figure 4c) electrical depression (forgetting) for 50 epochs. These noisy images were generated by superimposing the input current to the corresponding LED for each pixel with a zero mean white Gaussian random noise of different standard deviations ( $\sigma_p$ ). In the absence of forgetting (Figure 4b), the phototransistors which are expected to remain in the low conductance state also get randomly potentiated due to the noise, making it impossible to learn the pattern by the end of the 50 epochs. In contrast, when forgetting is enabled (Figure 4c), the random potentiations in the unintended phototransistors are compensated through regular electrical depression, allowing for the phototransistor array to learn the letter "T" despite the noisy illumination. As expected, learning takes longer under noisy conditions since forgetting reduces the learning rate. Nevertheless, this demonstration highlights the importance of forgetting in perceiving information obscured by noise and aids in the development of in-memory vision sensors that can seamlessly operate under environmental disturbances.

#### **CONCLUSION**

In summary, we have experimentally demonstrated a gamut of possibilities offered by a 2D-based in-memory optoelectronic

platform for next-generation machine intelligent systems. Direct analog learning from visual stimuli was experimentally demonstrated. Furthermore, the importance of forgetting in learning is shown using two examples: dynamic learning and learning under noisy conditions. Remarkably, the energy expenditure by our hardware vision platform was found to be in the ranges of tens of nanojoules for different learning and forgetting examples. Our findings highlight the benefits of inmemory computing and sensing for hardware acceleration of low-power and bioinspired machine intelligence.

#### **METHODS**

Film Growth. The monolayer MoS2 used in this study was obtained from the Pennsylvania State University 2D Crystal Consortium (2DCC).<sup>54</sup> It was deposited on an epi-ready 2" csapphire substrate by metal-organic chemical vapor deposition (MOCVD). An inductively heated graphite susceptor equipped with wafer rotation in a cold-wall horizontal reactor was used to achieve uniform monolayer deposition as previously described.<sup>69</sup> Molybdenum hexacarbonyl (Mo(CO)<sub>6</sub>) and hydrogen sulfide (H<sub>2</sub>S) were used as the precursors. Mo(CO)<sub>6</sub> was maintained at 10 °C and 950 Torr in a stainless-steel bubbler, which was used to deliver 0.036 sccm of the metal precursor for the growth, while 400 sccm of H<sub>2</sub>S was used. MoS<sub>2</sub> deposition was carried out at 1000 °C and 50 Torr in H<sub>2</sub> ambient, and monolayer growth was achieved in 18 min. The substrate was first heated to 1000 °C in H<sub>2</sub> and maintained for 10 min before the growth was initiated. After growth, the substrate was cooled in H<sub>2</sub>S to 300 °C to inhibit decomposition of the MoS<sub>2</sub> films.

Fabrication of Local Back-Gate Islands. To define the backgate island regions, a commercially bought substrate (285 nm SiO<sub>2</sub> on p<sup>++</sup>-Si) was spin-coated at 4000 rpm for 45 s with a bilayer photoresist consisting of Lift-Off-Resist (LOR 5A) and Series Photoresist (SPR 3012), which were baked at 185 and 95 °C, respectively. The bilayer photoresist was then exposed using a Heidelburg Maskless Aligner (MLA 150) to define the islands and developed using MF CD26 microposit, followed by a deionized (DI) water rinse. The local backgate island electrodes (20/50 nm TiN/Pt) were deposited using reactive sputtering. The photoresist was then removed using acetone and Photo Resist Stripper (PRS 3000) and cleaned using 2-propanol (IPA) and DI water. An atomic layer deposition (ALD) process was then implemented to grow 50 nm Al<sub>2</sub>O<sub>3</sub> uniformly across the entire substrate, including the island regions. To access the individual Pt back-gate electrodes, etch patterns were defined using the same bilayer photoresist (LOR 5A and SPR 3012) used previously. The bilayer photoresist was then again exposed using the MLA 150 and developed using MF CD26 microposit. The 50 nm Al<sub>2</sub>O<sub>3</sub> was subsequently dry etched using a BCl<sub>3</sub> reactive ion etch chemistry at 5 °C for a total of 80 s; this process was split into four 20 s etches to minimize heating in the substrate and thus ensure a uniform etch rate/depth. The photoresist was then removed to give access to the individual Pt electrodes.

**Film Transfer.** To fabricate the 2D phototransistors, the as-grown monolayer MoS<sub>2</sub> film was transferred from the sapphire growth substrate to the SiO<sub>2</sub>/p<sup>++</sup>-Si substrate with local back-gate islands using a PMMA (poly(methyl methacrylate)) assisted wet transfer process. PMMA 495 A6 resist was spun onto the growth substrate at 4000 rpm for 45 s and allowed to sit overnight to ensure good PMMA/MoS<sub>2</sub> adhesion. The edges of the spin-coated film were then scratched using a razor blade and the substrate was immersed into a 2 M NaOH solution kept at 90 °C. Capillary action served to draw the NaOH solution to the PMMA/substrate interface, separating the hydrophobic PMMA/MoS<sub>2</sub> from the hydrophilic sapphire substrate. Note that scratching the edges of the film served to aid this process via removing any PMMA beading that may have been formed at the edge of the substrate during spinning and shortening the distance for the solution to penetrate. The detached film was retrieved from the NaOH bath using a clean glass slide and rinsed three times in separate DI water baths (15 min each). It was then retrieved from the final

bath using the prepared  $SiO_2/p^{+2}$ -Si substrate with local back-gate islands and baked at 50 and 70 °C for 10 min each to remove moisture and promote adhesion. Finally, the PMMA supporting layer was removed using an acetone bath and the substrate was cleaned using IPA.<sup>70</sup>

Fabrication of Monolayer MoS<sub>2</sub> Phototransistors. To define the channel regions for the phototransistors, the sample was first spincoated with PMMA 950 A6 at 4000 rpm for 45 s and then baked at 180  $^{\circ}\text{C}$  for 90 s. Electron-beam (e-beam) lithography was used to pattern the resist, which was developed using a 1:1 mixture of 4methyl-2-pentanone (MIBK) and IPA for 60 s and pure IPA for 45 s. The defined channels were separated via dry-etching using a sulfur hexafluoride (SF<sub>6</sub>) reactive ion etch chemistry at 5 °C for 30 s. Following the etch step, the sample was rinsed in acetone for 30 min to remove the remaining photoresist, followed by an IPA bath to clean the sample. To define the source and drain contacts, sample was spincoated with methyl methacrylate (MMA) and baked at 150 °C for 90 s before applying PMMA A3, which was baked 185 °C for 90 s. Both resists were spun at 4000 rpm for 45 s. E-beam lithography was used to pattern the source and drain contacts, and development was again performed using a 1:1 mixture of MIBK and IPA for 60s and pure IPA for 45 s. Note that this development process allowed for the formation of a significant undercut in the bilayer resist, making subsequent metal deposition/liftoff easy. 40 nm of nickel (Ni) and 30 nm of gold (Au) were deposited using e-beam evaporation. Finally, lift-off of the evaporated material was performed by immersing the sample in acetone for 30 min and in IPA for 15 min. In the final design, each local back-gate island contained one phototransistor to allow for individual gate control.

**Electrical Characterization.** Electrical characterization of the fabricated devices was performed in a Lake Shore CRX-VF probe station under atmospheric conditions using a Keysight B1500A parameter analyzer.

#### **ASSOCIATED CONTENT**

#### Supporting Information

The Supporting Information is available free of charge at https://pubs.acs.org/doi/10.1021/acsnano.2c02906.

Memory-augmented reinforcement learning directly from the optical stimuli (MP4)

Forgetting of a learned "T" pattern at different rates enabled by  $V_{\rm erase}$  (MP4)

Time evolution of the heatmap of G during dynamic learning, i.e., sensing and storing the first image ("L") and gradually erasing it to store the new image ("T"), for different strengths of electrical depression obtained by using different  $V_{\rm erase}$  (MP4)

Time evolution of the heatmap of G measured at  $V_{BG} = 0$  V while learning from  $3 \times 3$  pixel noisy images of the letter "T" with and without electrical depression or forgetting for 50 epochs (MP4)

Benchmarking table of the emerging and conventional machine vision platforms, energy consumption in conventional vision platforms, material characterization of MOCVD grown monolayer MoS $_2$ , electrical performance of the phototransistor array, influence of  $V_{\rm write}$  in dark, postillumination transfer characteristics at different  $V_{\rm write}$ , influence of photogating effect for different wavelengths of light, device-to-device variation in photoresponse across the phototransistor array, gate-tunable adaptive sensing for scotopic and photopic conditions, band-diagrams illustrating the forgetting mechanism and finally the paired-pulse facilitation and paired-pulsed depression of a representative phototransistor (PDF)

#### **AUTHOR INFORMATION**

#### **Corresponding Author**

Saptarshi Das — Engineering Science and Mechanics, Materials Science and Engineering, Materials Research Institute, and Electrical Engineering and Computer Science, Penn State University, University Park, Pennsylvania 16802, United States; orcid.org/0000-0002-0188-945X; Email: sud70@psu.edu, das.sapt@gmail.com

#### **Authors**

- Akhil Dodda Engineering Science and Mechanics, Penn State University, University Park, Pennsylvania 16802, United States
- Darsith Jayachandran Engineering Science and Mechanics, Penn State University, University Park, Pennsylvania 16802, United States
- Shiva Subbulakshmi Radhakrishnan Engineering Science and Mechanics, Penn State University, University Park, Pennsylvania 16802, United States
- Andrew Pannone Engineering Science and Mechanics, Penn State University, University Park, Pennsylvania 16802, United States
- Yikai Zhang Engineering Science and Mechanics, Penn State University, University Park, Pennsylvania 16802, United States
- Nicholas Trainor Materials Science and Engineering, Penn State University, University Park, Pennsylvania 16802, United States
- Joan M. Redwing Materials Science and Engineering and Materials Research Institute, Penn State University, University Park, Pennsylvania 16802, United States; orcid.org/0000-0002-7906-452X

Complete contact information is available at: https://pubs.acs.org/10.1021/acsnano.2c02906

#### **Author Contributions**

S.D. conceived the idea and designed the experiments. A.D, D.J., A.P., Y.Z, S.S.R., and S.D. performed the experiments, analyzed the data, discussed the results, and agreed on their implications. N.T. and J.M.R. grew MOCVD MoS<sub>2</sub>. All authors contributed to the preparation of the manuscript.

#### Notes

Preprint: Akhil Dodda; Darsith Jayachandran; Shiva Subbulakshmi Radhakrishnan; Saptarshi Das. A Bio-inspired and Low-power 2D Machine Vision with Adaptive Machine Learning and Forgetting. **2021**, *Research Square*. 10.21203/rs. 3.rs-258246/v1 (02-24-2021).

The authors declare no competing financial interest.

#### **ACKNOWLEDGMENTS**

The work was supported by the Army Research Office (ARO) through Contract Number W911NF1920338 and the National Science Foundation (NSF) through CAREER Award under Grant Number ECCS-2042154. Authors also acknowledge the materials support from the NSF through 2D Crystal Consortium—Materials Innovation Platform (2DCCMIP) at the Pennsylvania State University under NSF cooperative agreement DMR-1539916.

#### REFERENCES

(1) Frisby, J. P.; Stone, J. V. Seeing: The Computational Approach to Biological Vision; MIT Press: Cambridge, 2010.

- (2) Silver, D.; Huang, A.; Madisson, J. C.; Guez, A.; Sifre, A.; Driessche, V.D. G.; Schrittwieser, J.; Antonoglou, I.; Pannershelvam, V.; Lanctot, M.; Dieleman, S.; Grewe, D.; Nham, J.; Kalchbrenner, N.; Sustskever, I.; Lillicrap, T.; Leach, M.; Kavukcuoglu, K.; Graepel, T.; Hassabis, D. Mastering the Game of Go with Deep Neural Networks and Tree Search. *Nature* **2016**, *529*, 484–489.
- (3) Lechner, M.; Hasani, R.; Amini, A.; Henzinger, A. T.; Rus, D.; Grosu, R. Neural Circuit Policies Enabling Auditable Autonomy. *Nature Machine Intelligence* **2020**, *2*, 642–652.
- (4) Hassoun, M. H. Fundamentals of artificial neural networks; MIT Press: Cambridge, 1995.
- (5) Liu, W.; Wang, Z.; Liu, X.; Zeng, N.; Liu, Y.; Alsaadi, E. F. A Survey of Deep Neural Network Architectures and their Applications. *Neurocomputing* **2017**, 234, 11–26.
- (6) Mishkin, D.; Sergievskiy, N.; Matas, J. Systematic Evaluation of Convolution Neural Network Advances on the Imagenet. *Computer Vision and Image Understanding* **2017**, *161*, 11–19.
- (7) Tavanaei, A.; Ghodrati, M.; Kheradpisheh, S. R.; Masquelier, T.; Maida, A. Deep Learning in spiking neural networks. *Neural Networks* **2019**, *111*, 47–63.
- (8) Davies, M.; Srinivasa, N.; Lin, T.-H.; Chinya, G.; Cao, Y.; Choday, S. H.; Dimou, G.; Joshi, P.; Imam, N.; Jain, S.; Liao, Y.; Lin, C.-K.; Lines, A.; Liu, R.; Mathaikutty, D.; McCoy, S.; Pau, A.; Tse, J.; Venkataraman, G.; Weng, Y.-H.; et al. Loihi: A Neuromorphic Manycore Processor With On-chip Learning. *IEEE Micro* **2018**, *38*, 82–99.
- (9) Merolla, P. A.; Arthur, V. J.; Alvarez-Icaza, R.; Cassidy, S. A.; Swada, J.; Akopyan, F.; Jackson, L.; Imam, N.; Guo, C.; Nakamura, Y.; Brezzo, B.; Vo, I.; Esser, K.; Appuswamy, R.; Taba, B.; Amir, A.; Flickner, D. M.; Risk, P. W.; Manohar, R.; Modha, S. D. A Million Spiking-Neuron Integrated Circuit with a Scalable Communication Network and Interface. *Science* **2014**, *345*, 668–673.
- (10) Pei, J.; Deng, L.; Song, S.; Zhao, M.; Zhang, Y.; Wu, S.; Wang, G.; Zou, Z.; Wu, Z.; He, W.; Chen, F.; Deng, N.; Wu, Y.; Yang, Z.; Ma, C.; Li, G.; Han, W.; Li, H.; Wu, H.; Zhao, R.; et al. Towards Artificial General Intelligence with Hybrid Tianjic Chip Architecture. *Nature* 2019, 572, 106–111.
- (11) Salahuddin, S.; Ni, K.; Datta, S. The Era of Hyper-scaling in Electronics. *Nature Electronics* **2018**, *1*, 442–450.
- (12) Ielmini, D.; Wong, H.-S. P. In-memory Computing with Resistive Switching Devices. *Nature Electronics* **2018**, *1*, 333–343.
- (13) Chai, Y. In-sensor Computing for Machine Vision. *Nature* **2020**, 579, 32–33.
- (14) Glackin, B.; McGinnity, T. M.; Maguire, L. P.; Wu, Q.; Belatreche, A. A Novel Approach for the Implementation of Large Scale Spiking Neural Networks on FPGA Hardware. *Proceeding of the 8th International Work-Conference on Artificial Neural Networks*, Jun 08–June 10, 2005, Barcelona, Spain; Cabestany, J., Prieto, A., Sandoval, F., Eds.; Springer-Verlag: Berlin, Heidelberg; pp 552–563.
- (15) Milo, V.; Pedretti, G.; Carboni, R.; Calderoni, A.; Ramaswamy, N.; Ambrogio, S.; Ielmini, D. Demonstration of Hybrid CMOS/RRAM Neural Networks with Spike time/rate-dependent Plasticity. *IEEE International Electron Devices Meeting (IEDM)*, San Francisco, USA, Dec 03–Dec 07, 2016; pp 16.18. 11–16.18. 14.
- (16) Wang, Z.; Joshi, S.; Savel'ev, S.; Song, W.; Midya, R.; Li, Y.; Rao, M.; Yan, P.; Asapu, S.; Zhuo, Y.; Jiang, H.; Lin, P.; Li, C.; Yoon, H. J.; Upadhay, K. N.; Zhang, J.; Hu, M.; Strachan, P. J.; Barnell, M.; Wu, Q.; et al. Fully Memristive Neural Networks for Pattern Classification with Unsupervised Learning. *Nature Electronics* **2018**, *1*, 137–145.
- (17) Al-Shedivat, M.; Naous, R.; Cauwenberghs, G.; Salama, K. N. Memristors Empower Spiking Neurons with Stochasticity. *IEEE journal on Emerging and selected topics in circuits and systems* **2015**, *5*, 242–253.
- (18) Kim, S.; Ishii, M.; Lewis, S.; Perri, T.; Brightsky, M.; Kim, W.; Jordan, R.; Burr, G. W.; Sosa, N.; Ray, A.; Han, J.-P.; Miller, K.; Hosokawa, K.; Lam, C. NVM Neuromorphic Core with 64k- cell (256-by-256) Phase Change Memory Synaptic Array with On-Chip Neuron Circuits for Continuous In-Situ Learning. *IEEE International*

- Electron Devices Meeting (IEDM), San Francisco, USA, Dec 05-Dec 09, 2015; pp 17.11. 11-17.11. 14.
- (19) Boybat, I.; Le Gallo, M.; Nandakumar, R. S.; Moraitis, T.; Parnell, T.; Tuma, T.; Rajemdran, B.; Leblebici, Y.; Sebastian, A.; Eleftheriou, E. Neuromorphic Computing with Multi-Memristive Synapses. *Nat. Commun.* **2018**, *9*, 1–12.
- (20) Ambrogio, S.; Ciocchini, N.; Laudato, M.; Milo, V.; Pirovano, A.; Fantini, P.; Lelmini, D. Unsupervised Learning by Spike Timing Dependent Plasticity in Phase Change Memory (PCM) Synapses. Frontiers in neuroscience 2016, 10, 56.
- (21) Yao, P. P.; Wu, H.; Gao, B.; Tang, J.; Zhang, Q.; Zhang, W.; Yang, J. J.; Qian, H. Fully Hardware-Implemented Memristor Convolutional Neural Network. *Nature* **2020**, *577*, 641–646.
- (22) Tanachutiwat, S.; Liu, M.; Wang, W. FPGA Based on Integration of CMOS and RRAM. *IEEE Transactions on Very Large Scale Integration (VLSI) Systems* **2011**, 19, 2023–2032.
- (23) Zhou, F.; Chai, Y. Near-Sensor and In-Sensor Computing. *Nature Electronics* **2020**, *3*, 664–671.
- (24) Kyuma, K.; Lange, E.; Ohta, J.; Hermanns, A.; Banish, B.; Oita, M. Artificial Retinas—Fast, Versatile Image Processors. *Nature* **1994**, 372, 197–198.
- (25) Ko, H. C.; Stoykovich, P. M.; Song, J.; Malyarchuk, V.; Choi, M. W.; Yu, C.-J.; Geddes, B. J., III.; Xiao, J.; Wang, S.; Huang, Y.; Rogers, A. J. A Hemispherical Electronic Eye Camera Based on Compressible Silicon Optoelectronics. *Nature* **2008**, 454, 748–753.
- (26) Ishikawa, M.; Ogawa, K.; Komuro, T.; Ishii, I. A CMOS Vision Chip with SIMD Processing Element Array for 1 ms Image Processing. 1999 IEEE International Solid-State Circuits Conference. Digest of Technical Papers, First ed.; San Francisco, USA, Feb 17, 1999; pp 206–207.
- (27) Rodriguez-Vazquez, A.; Fernandez-Berni, J.; Lenero-Bardallo, J. A.; Vornicu, I.; Carmona-Galan, R. CMOS Vision Sensors: Embedding Computer Vision at Imaging Front-Ends. *IEEE Circuits and Systems Magazine* **2018**, *18*, 90–107.
- (28) Gu, L.; Poddar, S.; Lin, Y.; Long, Z.; Zhang, D.; Zhang, Q.; Shu, L.; Qiu, X.; Kam, M.; Javey, A.; Fan, Z. A Biomimetic Eye with A Hemispherical Perovskite Nanowire Array Retina. *Nature* **2020**, *581*, 278–282.
- (29) Zhou, F.; Zhou, Z.; Chen, J.; Chou, H. T.; Wang, J.; Zhang, N.; Lin, Z.; Yu, S.; Kang, J.; Wong, P. H.-S.; Chai, Y. Optoelectronic Resistive Random Access Memory for Neuromorphic Vision Sensors. *Nature Nanotechnol.* **2019**, *14*, 776–782.
- (30) Chen, S.; Lou, Z.; Chen, D.; Shen, G. An Artificial Flexible Visual Memory System Based on an UV-Motivated Memristor. *Adv. Mater.* **2018**, *30*, 1705400.
- (31) Kwon, M. S.; Cho, W. S.; Kim, M.; Heo, S. J.; Kim, Y.-H.; Park, K. S. Environment-Adaptable Artificial Visual Perception Behaviors Using a Light-Adjustable Optoelectronic Neuromorphic Device Array. *Adv. Mater.* **2019**, *31*, No. 1906433.
- (32) Zhou, F.; Zhou, Z.; Chen, J.; Chou, H. T.; Wang, J.; Zhang, N.; Lin, Z.; Yu, S.; Kang, J.; Wong, P. H.-S.; Chai, Y. Optoelectronic Resistive Random Access Memory for Neuromorphic Vision Sensors. *Nature Nanotechnol.* **2019**, *14*, 776–782.
- (33) Dai, S.; Wu, X.; Liu, D.; Chu, Y.; Wang, K.; Yang, B.; Huang, J. Light-Stimulated Synaptic Devices Utilizing Interfacial Effect of Organic Field-Effect Transistors. ACS Appl. Mater. Interfaces 2018, 10, 21472–21480.
- (34) Yin, L.; Huang, W.; Xiao, R.; Peng, W.; Zhu, Y.; Zhang, Y.; Pi, X.; Yang, D. Optically Stimulated Synaptic Devices Based on the Hybrid Structure of Silicon Nanomembrane and Perovskite. *Nano Lett.* **2020**, 20, 3378–3387.
- (35) Hou, Y.-X.; Li, Y.; Zhang, Z.-C.; Li, J.-Q.; Qi, D.-H.; Chen, X.-D.; Wang, J.-J.; Yao, B.-W.; Yu, M.-X.; Lu, M.-X.; Zhang, J. Large-Scale and Flexible Optical Synapses for Neuromorphic Computing and Integrated Visible Information Sensing Memory Processing. *ACS Nano* **2021**, *15*, 1497–1508.
- (36) Hong, S.; Choi, H. S.; Park, J.; Yoo, H.; Oh, Y. J.; Hwang, E.; Yoon, H. D.; Kim, S. Sensory Adaptation and Neuromorphic

- Phototransistors Based on  $CsPb(Br_{1-x}I_x)_3$  Perovskite and  $MoS_2$  Hybrid Structure. ACS Nano **2020**, 14, 9796–9806.
- (37) Mennel, L.; Symonowicz, J.; Watcher, S.; Polyushki, K. D.; Molina-Mendoza, J. A.; Mueller, T. Ultrafast Machine Vision with 2D Material Neural Network Image Sensors. *Nature* **2020**, *579*, 62–66.
- (38) Wang, Q. H.; Kalantar-Zadeh, K.; Kis, A.; Coleman, N. J.; Strano, S. M. Electronics and Optoelectronics of Two-Dimensional Transition Metal Dichalcogenides. *Nat. Nanotechnol.* **2012**, *7*, 699.
- (39) Das, S.; Robinson, J. A.; Dubey, M.; Terrones, H.; Terrones, M. Beyond Graphene: Progress in Novel Two-Dimensional Materials and van der Waals Solids. *Annu. Rev. Mater. Res.* **2015**, *45*, 1–27.
- (40) Hong, S.; Cho, H.; Kang, B. H.; Park, K.; Akinwande, D.; Kim, H. J.; Kim, S. Neuromorphic Active Pixel Image Sensor Array for Visual Memory. *ACS Nano* **2021**, *15*, 15362–15370.
- (41) Smets, Q.; Arutchelvan, G.; Jussot, J.; Verreck, D.; Asselberghs, I.; Mehta, A. N.; Gaur, A.; Lin, D.; El Kazzi, S.; Groven, B.; Caymax, M.; Radu, I. Ultra Scaled MOCVD MoS<sub>2</sub> MOSFETs with 42nm Pitch and 250μA/μm Drain Current. *IEEE International Electron Devices Meeting (IEDM)*, San Francisco, USA, Dec 07–Dec 11, 2019; pp 23.22. 21–23.22. 24 (IEEE).
- (42) Migliato Marega, G.; Zhao, Y.; Avsar, A.; Wang, Z.; Tripathi, M.; Radenovic, A.; Kis, A. Logic-in-memory based on An Atomically Thin Semiconductor. *Nature* **2020**, *587*, 72–77.
- (43) Jayachandran, D.; Oberoi, A.; Sebastian, A.; Choudhury, T. M.; Shankar, B.; Redwing, J. M.; Das, S. A Low-Power Biomimetic Collision Detector Based on an In-Memory Molybdenum Disulfide Photodetector. *Nature Electronics* **2020**, *3*, 646–655.
- (44) Jang, H.; Liu, C.; Hinton, H.; Lee, M.-H.; Kim, H.; Seol, M.; Shin, H.-J.; Park, S.; Ham, D. An Atomically Thin Optoelectronic Machine Vision Processor. *Adv. Mater.* **2020**, 32, No. 2002431.
- (45) Seo, S.; Jo, S.-H.; Kim, S.; Shim, J.; Oh, S.; Kim, J.-H.; Heo, K.; Choi, J.-W.; Choi, C.; Oh, S.; Kuzum, D.; Wong, H-S. P.; Park, J.-H. Artificial Optic-Neural Synapse for Colored and Color-Mixed Pattern Recognition. *Nat. Commun.* **2018**, *9*, 5106.
- (46) Choi, C.; Lenn, J.; Kim, M. S.; Taqieddin, A.; Cho, C.; Cho, K. W.; Lee, G. J.; Seiung, H.; Bae, H. J.; Song, Y. M.; Hyeon, T.; ALuru, R. N.; Nam, S.; Kim, D.-H. Curved Neuromorphic Image Sensor Array Using a MoS<sub>2</sub>-Organic Heterostructure Inspired by The Human Visual Recognition System. *Nat. Commun.* **2020**, *11*, 5934.
- (47) Hou, X.; Liu, C.; Ding, Y.; Liu, L.; Wang, S.; Zhou, P. A Logic-Memory Transistor with the Integration of Visible Information Sensing-Memory-Processing. *Advanced Science* **2020**, *7*, 2002072.
- (48) Gravitz, L. The Importance of Forgetting. *Nature* **2019**, *571*, S12–S14.
- (49) Dodda, A.; Oberoi, A.; Sebastian, A.; Choudhury, T. H.; Redwing, J. M.; Das, S. Stochastic Resonance in MoS2 Photodetector. *Nat. Commun.* **2020**, *11*, 4406.
- (50) Sebastian, A.; Pendurthi, R.; Choudhury, T. H.; Redwing, J. M.; Das, S. Benchmarking Monolayer MoS<sub>2</sub> and WS<sub>2</sub> Field-Effect Transistors. *Nat. Commun.* **2021**, *12*, 693.
- (51) Rai, A.; Valsaraj, A.; Movva, H. C. P.; Roy, A.; Ghosh, R.; Sonde, S.; Kang, S.; Chang, J.; Trivedi, T.; Dey, R.; Guchhait, S.; Larentis, S.; Register, L. F.; Tutuc, E.; Banerjee, S. K. Air Stable Doping and Intrinsic Mobility Enhancement in Monolayer Molybdenum Disulfide by Amorphous Titanium Suboxide Encapsulation. *Nano Lett.* **2015**, *15*, 4329–4336.
- (52) English, C. D.; Smithe, K. K. H.; Xu, R. L.; Pop, E. Approaching Ballistic Transport in Monolayer MoS<sub>2</sub> Transistors with Self-aligned 10 nm Top Gates. *IEEE International Electron Devices Meeting (IEDM)*, San Francisco, USA, Dec 03–Dec 07, 2016; pp 5.6.1–5.6.4.
- (53) Price, K. M.; Schauble, K. E.; McGuire, F. A.; Farmer, D. B.; Franklin, A. D. Uniform Growth of Sub-5-Nanometer High-κ Dielectrics on MoS<sub>2</sub> Using Plasma-Enhanced Atomic Layer Deposition. *ACS Appl. Mat & Interf* **2017**, *9*, 23072–23080.
- (54) 2D Crystal Consortium. *List of Thin Film Samples Available*; www.mri.psu.edu/2d-crystal-consortium/user-facilities/thin-films/list-thin-film-samples-available, Mar 1, 2016.
- (55) Kang, K.; Xie, S.; Huang, L.; Han, Y.; Huang, P. Y.; Mak, K. F.; Kim, C.-J.; Muller, D.; Park, J. High-Mobility Three-Atom-Thick

Semiconducting Films With Wafer-Scale Homogeneity. *Nature* 2015, 520, 656.

- (56) Wachter, S.; Polyushkin, D. K.; Bethge, O.; Mueller, T. A Microprocessor Based on A Two-Dimensional Semiconductor. *Nat. Commun.* **2017**, *8*, 14948.
- (57) Polyushkin, D. K.; Watcher, S.; Mennel, L.; Paur, M.; Paliy, M.; Iannaccone, G.; Fiori, G.; Neumaier, D.; Canto, B.; Mueller, T. Analogue Two-Dimensional Semiconductor Electronics. *Nature Electronics* **2020**, *3*, 486–491.
- (58) Gao, Q.; Zhang, Z.; Xu, X.; Song, J.; Li, X.; Wu, Y. Scalable High-Performance Radio Frequency Electronics Based on Large Domain Bilayer MoS2. *Nat. Commun.* **2018**, *9*, 4778.
- (59) Kim, S. J.; Choi, K.; Lee, B.; Kim, Y.; Hong, B. H. Materials for Flexible, Stretchable Electronics: Graphene and 2D Materials. *Annu. Rev. Mater. Res.* **2015**, *45*, 63–84.
- (60) Torrisi, F.; Coleman, N. J. Electrifying Inks with 2D Materials. *Nat. Nanotechnol.* **2014**, *9*, 738–739.
- (61) Das, S.; Dodda, A.; Das, S. A Biomimetic 2D Transistor for Audiomorphic Computing. *Nat. Commun.* **2019**, *10*, 3450.
- (62) Sebastian, A.; Pannone, A.; Radhakrishnan, S. S.; Das, S. Gaussian Synapses for Probabilistic Neural Networks. *Nat. Commun.* **2019**, *10*, 1–11.
- (63) Arnold, A. J.; Razavieh, A.; Nasr, J. R.; Schulman, D. S.; Eichfeld, C. M.; Das, S. Mimicking Neurotransmitter Release in Chemical Synapses *via* Hysteresis Engineering in MoS<sub>2</sub> Transistors. *ACS Nano* **2017**, *11*, 3110–3118.
- (64) Dodda, A.; Das, S. Demonstration of Stochastic Resonance, Population Coding, and Population Voting Using Artificial MoS<sub>2</sub> Based Synapses. *ACS Nano* **2021**, *15*, 16172–16182.
- (65) Abbott, L. F.; Nelson, S. B. Synaptic Plasticity: Taming the beast. *Nature Neuroscience* **2000**, *3*, 1178–1183.
- (66) Shepherd, J. D.; Huganir, R. L. The Cell Biology of Synaptic Plasticity: AMPA Receptor Trafficking. *Annu. Rev. Cell Dev. Biol.* **2007**, 23, 613–643.
- (67) Zhuang, C.; Yan, S.; Nayebi, A.; Schrimpf, M.; Frank, C. M.; Dicarlo, J. J.; Yamins, D. L. K. Unsupervised Neural Network Models of The Ventral Visual Stream. *Proc. Natl. Acad. Sci. U. S. A.* **2021**, *118*, 118.
- (68) Wang, C.-Y.; Liang, S.J.; Wang, S.; Wang, P.; Li, Z.; Wang, Z.; Gao, A.; Pan, C.; Liu, C.; Liu, J.; Yang, H.; Liu, X.; Song, W.; Wang, C.; Cheng, B.; Wang, X.; Chen, K.; Wang, Z.; Watanabe, K.; Taniguchi, T.; et al. Gate-Tunable Van der Waals Heterostructure for Reconfigurable Neural Network Vision Sensor. *Science Advances* 2020, 6, No. eaba6173.
- (69) Xuan, Y.; Jain, A.; Zafar, S.; Lotfi, R.; Nayir, N.; Wang, Y.; Choudhury, T. H.; Wright, S.; Fereca, J.; Rosenbaum, L.; Redwing, J. M.; Crespi, V.; Van Duin, A. C. T. Multi-Scale Modeling of Gas-Phase Reactions in Metal-Organic Chemical Vapor Deposition Growth of WSe<sub>2</sub>. J. Crys. Grow. 2019, 527, 125247.
- (70) Sebastian, A.; Zhang, F.; Dodda, A.; May-Rawdling, D.; Liu, H.; Zhang, T.; Terrones, M.; Das, S. Electrochemical Polishing of Two-Dimensional Materials. *ACS Nano* **2019**, *13*, 78–86.

### **□** Recommended by ACS

## Second-Order Conditioning Emulated in an Artificial Synaptic Network

Bharath Bannur, Giridhar U. Kulkarni, et al.

MARCH 29, 2022

ACS APPLIED ELECTRONIC MATERIALS

READ 🗹

#### **Resonance for Analog Recurrent Neural Network**

Yurui Qu, Zongfu Yu, et al.

APRIL 27, 2022

ACS PHOTONICS

READ **C** 

#### Multimodal Artificial Neurological Sensory–Memory System Based on Flexible Carbon Nanotube Synaptic Transistor

Haochuan Wan, Chuan Wang, et al.

SEPTEMBER 02, 2021

ACS NANO

READ **C** 

# Bienenstock-Cooper-Munro Learning Rule Realized in Polysaccharide-Gated Synaptic Transistors with Tunable Threshold

Jianmiao Guo, Feng Huang, et al.

OCTOBER 26, 2020

ACS APPLIED MATERIALS & INTERFACES

READ **C** 

Get More Suggestions >